Deep Learning-Assisted Focused Ion Beam Nanofabrication

Oleksandr Buchnev[*,§], *James A. Grant-Jacob*[*,§], *Robert W. Eason*[*], *Nikolay I. Zheludev*[*,†], *Ben Mills*[*,‡], *and Kevin F. MacDonald*[*,‡]

* Optoelectronics Research Centre, University of Southampton,
Highfield, Southampton, SO17 1BJ, UK

† Centre for Disruptive Photonic Technologies & The Photonics Institute,
SPMS, Nanyang Technological University Singapore, 637371, Singapore

‡ E-mail: b.mills@soton.ac.uk; kfm@orc.soton.ac.uk

ABSTRACT: Focused Ion Beam (FIB) milling is an important rapid prototyping tool for micro and nanofabrication, device and materials characterization. It allows the manufacturing of arbitrary structures in a wide variety of materials but establishing the process parameters for a given task is a multi-dimensional optimization challenge, usually addressed through time-consuming, iterative trial-and-error. Here, we show that deep learning from prior experience of manufacturing can predict the post-fabrication appearance of structures manufactured by focused ion beam (FIB) milling with accuracy >96% over a range of ion beam parameters, taking account of instrument- and target-specific artefacts. With predictions taking only a few milliseconds, the methodology may be deployed in near real-time to expedite optimization and improve reproducibility in FIB processing.

KEYWORDS: *nanofabrication, deep learning, focused ion beam milling*

Introduction

Focused Ion Beam (FIB) milling is a 'direct-write' fabrication technique based on the removal of material from a target surface by a focused beam of ions[1, 2]. It can etch features with nanometric resolution into almost any metal, semiconductor, dielectric, or biomaterial. As such, it has become a standard tool in semiconductor (i.e. microelectronics) manufacturing, rapid prototyping and nano/bio/materials research. The end result of any FIB milling process is a complex function of beam current, spot size, scan pattern, target material characteristics and design geometry, especially the aspect ratio of the pattern. Producing a comprehensive analytical model that describes the physical processes occurring during milling is consequently an intractable problem. Time-consuming, trial-and-error testing is therefore invariably required to establish optimal process parameters for achieving the intended outcome of a given milling operation on a given target.

Computational, numerical approaches to simulating FIB milling are typically based upon Monte Carlo modelling of ion-atom interactions, and string or level set methods to track surface propagation over time[3-8]. They can reproduce 2D and 3D cross-sectional profiles of FIB milled trenches or holes in certain materials but are mathematically complex and require again detailed knowledge of numerous parameters, such as ion energy and angle of incidence to a target surface, ion flux, ion beam spot size and intensity profile, dwell time and raster step size, atomic mass and physical form (e.g., mono/polycrystalline; amorphous) of target, etc. Deep learning offers an alternative approach whereby milling outcomes for arbitrary nano/microstructural geometries in any target medium can be accurately predicted by a suitably trained neural network.

Deep learning is revolutionizing scientific research[9-14], due to its aptitude for pattern recognition and the capability to empirically establish the functional algorithms of complex systems[15]. For example, it has been shown that deep learning can improve laser machining processes[16-18], including through the provision of feedback for real-time process control[19-21]. Here we show that deep learning can be used to simulate the post-fabrication appearance of structures manufactured by focused ion beam (FIB) milling in the 2D projection of a scanning electron microscope image, as a very good (almost invariably the first, in-situ) indicator of process accuracy and quality. With

predictions generated on millisecond timescales, the approach can be deployed to reproducibility and precision in FIB manufacturing processes.

Results and Discussion

We demonstrate that deep learning can assist in predicting the post-fabrication appearance of two-dimensional binary patterns FIB milled into a gold thin film (Fig. 1). Such structures are widely used in nanophotonic and metamaterial devices, seeded growth of nanostructures, and a range of other applications[22-26].

In this work we used an FEI Helios Nanolab 600 DualBeam FIB/SEM system, which incorporates a gallium ion gun with a milling resolution of ~20 nm and a field-emission scanning electron microscope (SEM) with imaging resolution down to ~1 nm. In all cases, the binary patterns (i.e. comprising areas either exposed or not exposed to the ion beam) were fabricated by raster scanning

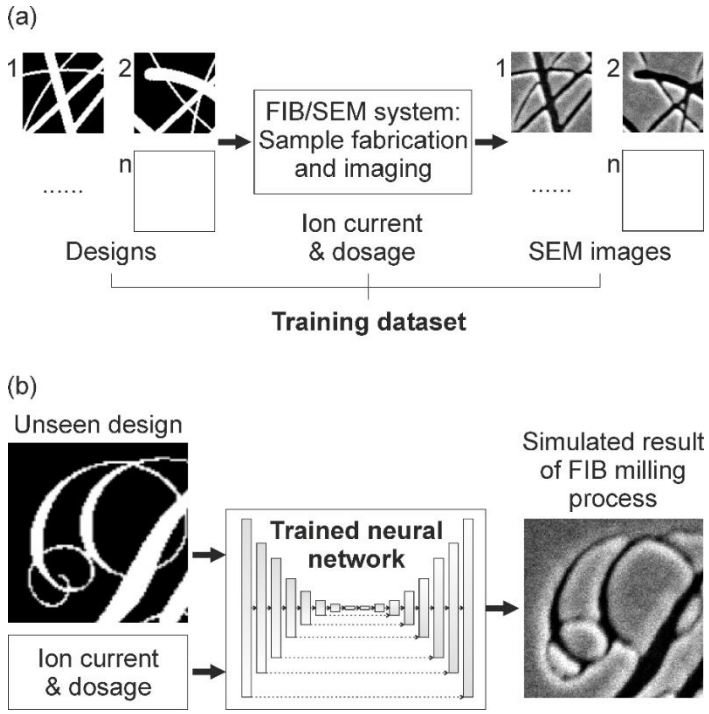

Figure 1. Deep learning simulation of FIB milling. (a) The neural network is trained on a set of binary design patterns, corresponding SEM images of samples manufactured by FIB milling, and detail of the ion beam parameters used in their production. (b) The trained network is then able to accurately predict the outcome of FIB milling processes – the expected post-fabrication appearance of samples in SEM imaging – for previously unseen designs.

the ion beam in lines running from left to right (as seen in images below), stepped from top to bottom. This consistency of procedure, as will be demonstrated, is essential to the effective application of deep learning to prediction of process outcomes.

We first demonstrate the use of deep learning to relate the appearance of a simple geometric design - an isolated sub-micron chevron shape (Fig. 2a) – in an SEM image to the ion beam parameters employed in its fabrication. To create a training and testing dataset we milled the chevron shape

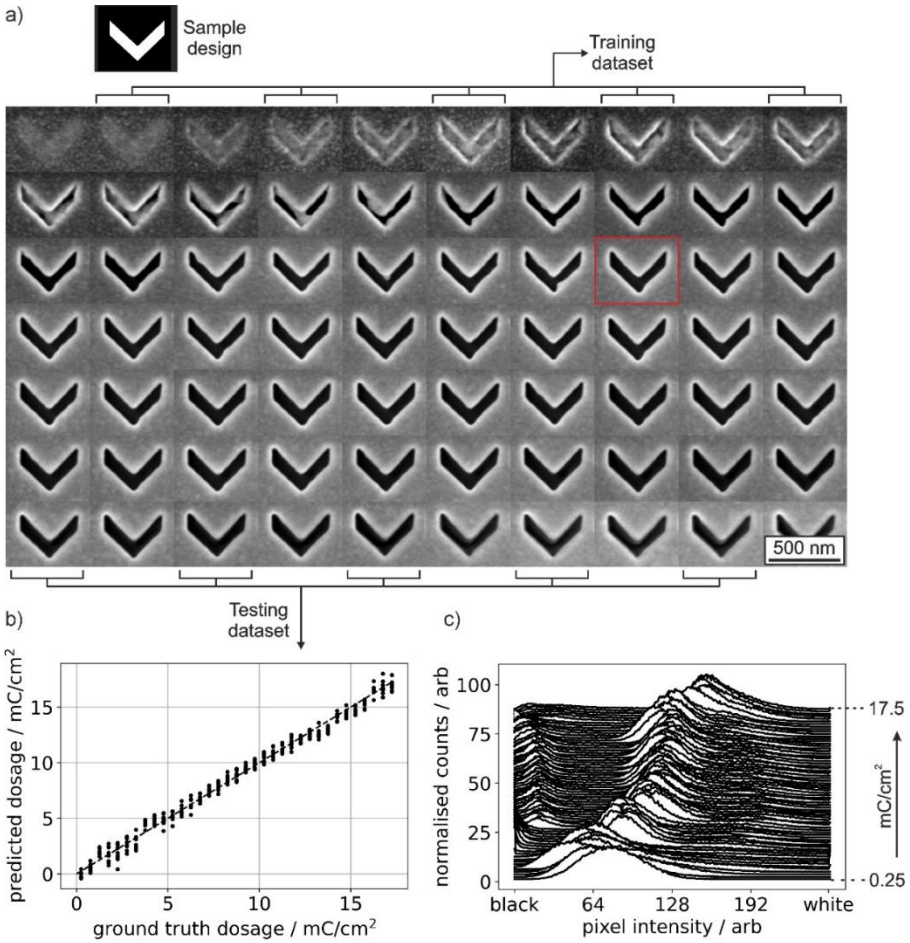

Figure 2. (a) SEM images of one of nine sets of 70 chevron structures milled into a 50 nm thick gold film with ion beam dosages ranging from 0.25 [top left] to 17.5 mC/cm^2 [bottom-right]. The chevron design [i.e. input pattern for FIB milling] is shown above. Half of the images [as labelled] are used for neural network training; the other half for testing [panel (b)]. Later experiments [see Fig. 3-5] use a dose of 7 mC/cm^2, as per the chevron image outlined in red. b) Correlation between trained neural network predictions of mC/cm^2 milling dosage from chevron SEM images in the testing set and actual [ground truth] dosage used in fabrication of the sample. c) Histograms of pixel intensity for the set of chevron SEM images shown in panel (a) [peak count number amplitudes are normalized for clarity].

into a 50 nm thick (thermally evaporated) gold film nine times at seventy different FIB dosage settings, ranging from 0.25 to 17.5 mC/cm^2 in 0.25 mC/cm^2 steps, with a fixed ion beam current of 9.8 pA, creating 630 separate chevron elements. Figure 2a illustrates how the chevron's appearance in SEM imaging changes with increasing ion beam dosage, from top-left (where it is insufficient for the design to penetrate the full thickness of the gold film) to bottom right.

A convolutional neural network (CNN – see Supplementary Information) was trained using one half of the experimental SEM image dataset and tested on the other. Figure 2b shows experimental versus predicted dose for the 315 images in the testing set - there is a clear correlation, with a root mean squared error of 0.52 mC/cm^2. Whilst the method of dosage identification established by the neural network cannot be known, the set of pixel intensity histograms in Fig. 2c provides some insight to the statistical differences among SEM images of chevrons milled with different ion beam settings: There is a clear trend towards higher pixel intensities (i.e. brighter images) with increasing dose, and a small peak at low pixel intensity emerges when the dose is high enough for the design to be milled through the full thickness of the gold film, exposing the silicon substrate (which appears black in SEM images).

We next addressed the more complex challenge of simulating the FIB milling process for arbitrary patterns – aiming to accurately predict the outcome, i.e. what a sample will look like in an SEM image (as a strong indicator of process accuracy and quality), for previously unseen designs.

This simulation is performed by a conditional generative adversarial network (cGAN)[27-29] trained on a set of 59 binary design and corresponding sample SEM images (Fig. 3 - see Supplementary Information for detail of the adversarial configuration used in network training). Designs comprised randomly generated arrangements of straight line and circle segments (each of random length and line width), so as to collectively include a very wide variety of straight/curved edges and intersection angles, at assorted orientations to the ion beam raster scan direction. They were fabricated using one of four ion gun aperture (beam current) settings with a fixed dosage of 7 mC/cm^2 (sufficient to consistently penetrate the gold film without excessive over-milling of the substrate – as illustrated for the chevrons in Fig. 2a by the highlighted SEM image).

The trained network was subsequently asked to predict what SEM images of previously unseen binary designs would look like, were they to be fabricated with certain ion beam settings. Figure 4 shows a comparison between predicted and actual FIB milling process outcomes for the

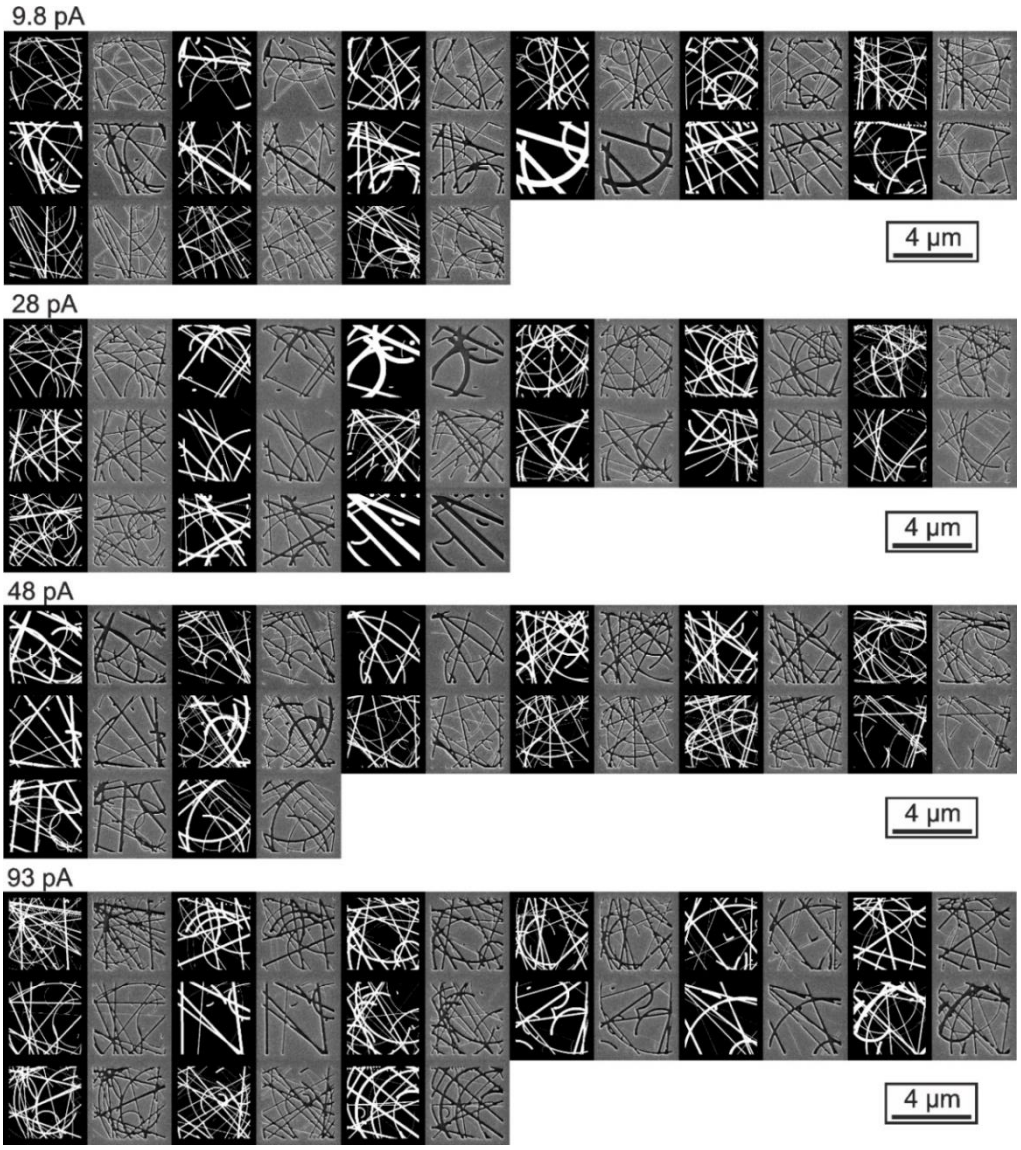

Figure 3. Training dataset for FIB process simulation by a neural network, showing randomly generated binary designs (left of each pair) and corresponding FIB-milled sample SEM images (right), grouped by the ion beam current setting employed in sample fabrication.

acronymic logo of the UK's Engineering and Physical Sciences Research Council at sub-micron font size (character height ~360 nm). The accuracy of neural network predictions is evaluated here in terms of the mean magnitude of pixel intensity difference between predicted and real sample SEM images, above the noise level intrinsic to SEM imaging (i.e. of an unstructured surface). The correlation is extremely good, with the network achieving >96% accuracy over the entire trained order-of-magnitude ion beam current range: with increasing beam current, for example, increased

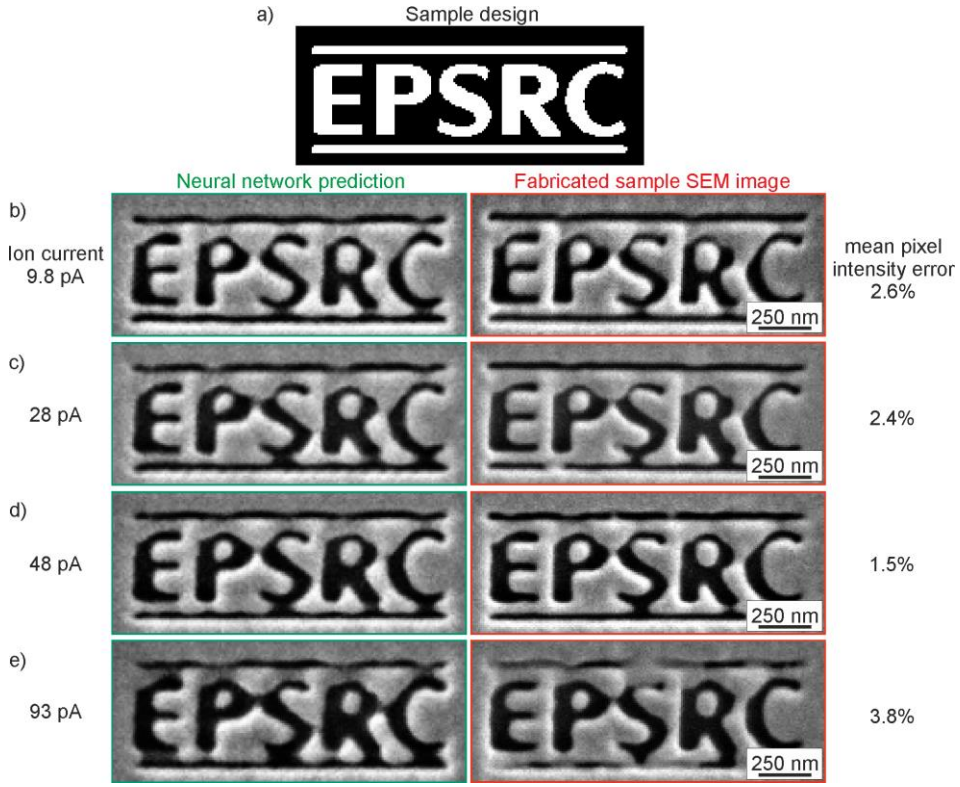

Figure 4. Comparison between neural network-predicted [left column] and actual FIB milled sample SEM images [right] for the EPSRC logo – the binary design shown in (a), for a selection of ion beam current [aperture] settings: b) 9.8, c) 28, d) 48, e) 93 pA.

over-milling of the design is correctly predicted, such as in the gradual disappearance of the gap between the letters P and S. Remarkably, the network correctly predicts defective shaping in the top left corner of each letter that is consistently observed across all ion current settings. This is an artefact (likely related to ion beam alignment and/or raster scan pattern) that has been identified by the network as systematically present within the training dataset, while being imperceptible there to the human eye. The network has then accounted for this process artefact in its predictions of milling outcomes.

Figure 5 presents a more detailed, quantitative comparison between predicted and experimental images of our departmental “Light” logo, which features an assortment of curved and intersecting lines of varying width, akin to the training patterns. Prediction accuracy for the image as a whole image (i.e. evaluated as above, as the mean magnitude of pixel intensity difference between predicted and real sample SEM images, above the unstructured surface noise floor) is >98%. Cross-sectional pixel intensity profiles through corresponding parts of the design provide insight

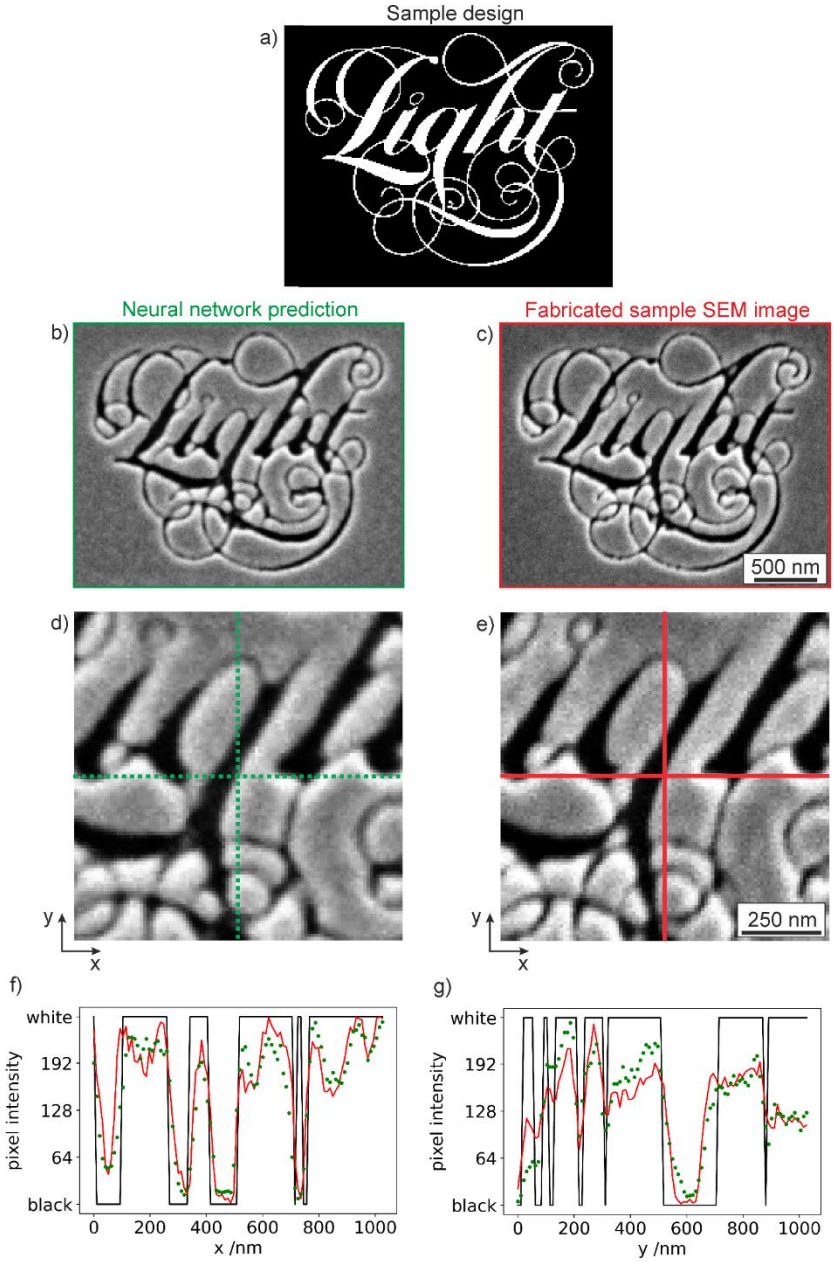

Figure 5. (a) Binary design image of the Optoelectronics Research Centre's "Light" logo. (b) Neural network-predicted [left column] and (c) actual FIB milled sample SEM images of the logo, for an ion beam current setting of 9.8 pA. (d, e) Enlarged detail of central 100 × 100 pixel regions of (b) and (c). (f, g) Pixel intensity profiles along the (f) horizontal and (g) vertical green and red lines in panels (d) and (e), plotted in those colors [i.e. network-predicted profiles in green; fabricated sample SEM image profiles in red]. The overlaid black lines are the corresponding binary design profiles [inverted with respect to (a) as white areas of the design are milled, becoming black in experimental samples].

to the network's success in meeting its objective: It is tasked, in essence, with mapping the binary (input) profiles denoted by black lines in Fig. 5f, g to the experimental sample profiles from SEM

imaging (plotted in red), with a success metric being the difference between the latter and the dotted green lines, which show network-generated profiles. Even though the transformation is both highly nonlinear and dependent on the surrounding pixel intensities in all directions, there is strong correspondence over a range of feature sizes in the design between predicted and experimental sample profiles. Improvements in this correlation may be achieved through optimization of the training hyperparameters (e.g. number of epochs and learning rate – see further detail in Supplementary Information) and/or inclusion of additional training data, for example to address circumstances in which the network's predictive capability is found to be weak.

Conclusion

In summary, we have shown that a neural network can accurately predict the post-fabrication appearance in scanning electron microscope images of samples manufactured by focused ion beam milling, over a wide range of sample design geometries (arbitrary micro/nanostructural feature shapes and dimensions), and ion beam parameters (current and per-unit-area dosage). With each prediction taking only a few tens of milliseconds, this capability can significantly reduce the time and the number of experimental dose-test iterations required in the development and optimization of new FIB processes It can also be employed to rapidly evaluate the impact of design or process parameter modifications, and to maintain performance (i.e. consistency of outcomes from established processes) against ageing of the ion source and ion gun beam apertures, thereby increasing the useful lifetime of said components, particularly where employed in highly repetitive (e.g. cross-sectional characterization) tasks. Predictions are sufficiently accurate as to include instrument- and/or target material-specific artefacts. These cannot be accounted for in numerical or analytical approaches to simulating FIB milling. That they may be imperceptible to the human eye in training samples, or may might appear as random (e.g. re-deposition) defects in isolated test samples, raises the prospect that such networks could be deployed for early fault (e.g. beam alignment, aperture damage) detection and identification.

In this proof-of-principle study we trained a network to simulate a specific type of FIB milling task on a specific target medium, while varying ion current and dosage (i.e. keeping all other system parameters constant). In practice, one would train the network to the task(s) at hand (i.e. according to application context, such as in semiconductor wafer-based device characterization or

in nanofabrication for plasmonics research), on a relevant variety of target materials, and with a full range of substrate and system metadata (e.g. film deposition methods, rates and thickness, crystal orientations, etc.; ion current, dosage, raster scan pattern, number of repetitions, ion source and aperture age, etc.). In this way, the network would accrue an 'understanding' of the complex relationships among the numerous sample and system parameters that affect process outcomes.

Indeed, we would argue that there is considerable scope for functional enhancement of FIB/SEM systems, as integrated micro/nano-manufacturing and sample characterization (i.e. fabrication and in-situ diagnostic) platforms, through the application of machine learning methodologies. For example, we (as chemists, physicists, and materials scientists; and as users of FIB milling tools) understand that families of materials have similar physical properties derived from similarities in composition and atomic/molecular structure. Neural networks are highly effective at discovering such patterns in complex, multi-dimensional datasets can similarly 'learn' that there are relationships among types of material[30-34]. Thus, a network trained on say, conductive oxide compositions A, B, C, and D, may 'intuitively' perform very well in application to previously unseen composition E, if told simply that it is another conductive oxide – i.e. it would not require dedicated training on every new target material encountered. It is also possible that neural networks trained for applications to FIB process development and control could contribute to new scientific understanding of the milling process (i.e. ion beam-target interactions)[15, 35-37].

ASSOCIATED CONTENT

Supporting Information. Contains further detail on: Convolutional Neural Network (CNN) and Conditional Generative Adversarial Network (cGAN) architectures.

Data availability Following a period of embargo, the data from this paper will be available from the University of Southampton ePrints research repository: https://doi.org/10.5258/soton/D2030.

AUTHOR INFORMATION

Corresponding Authors

Ben Mills − https://orcid.org/0000-0002-1784-1012; Email: b.mills@soton.ac.uk

Kevin F. MacDonald − orcid.org/0000-0002-3877-2976; Email: kfm@orc.soton.ac.uk

Authors

Oleksandr Buchnev − orcid.org/0000-0001-6161-2797

James A. Grant-Jacob − orcid.org/0000-0002-4270-4247

Robert W. Eason – orcid.org/0000-0001-9704-2204

Nikolay I. Zheludev − orcid.org/0000-0002-1013-6636

Author Contributions

NIZ, KFM, and BM conceived the idea and methodology for the study. § OB and JAGJ contributed equally to this work, respectively manufacturing FIB samples and training the neural networks. All authors discussed and analyzed the results, and contributed to writing the paper. KFM and BM supervised the work.

Notes

The authors declare no competing financial interests.

ACKNOWLEDGMENTS

This work was supported by the Engineering and Physical Sciences Research Council, UK [grant numbers EP/N03368X/1, EP/T026197/1, EP/M009122/1, EP/T02643X/1, and EP/N00762X/1], and the Singapore Ministry of Education [MOE2016-T3-1-006]. We acknowledge the NVIDIA Academic Hardware Grant Program for donation of the Nvidia Titan Xp GPU.

REFERENCES

1. Langford, R. M.; Nellen, P. M.; Gierak, J.; Fu, Y., Focused Ion Beam Micro- and Nanoengineering. *MRS Bull.* **2007,** 32, (5), 417-423.
2. Orloff, J.; Swanson, L.; Utlaut, M., *High Resolution Focused Ion Beams: FIB and its Applications*. Springer: Boston, MA, 2003.

3. Müller, K.; Weigmann, U.; Burghause, H., Simulation of focused ion beam milling. *Microelectron. Eng.* **1986,** 5, (1-4), 481-489.

4. Osher, S.; Fedkiw, R. P., Level Set Methods: An Overview and Some Recent Results. *J. Comput. Phys.* **2001,** 169, (2), 463-502.

5. Kim, H.-B.; Hobler, G.; Steiger, A.; Lugstein, A.; Bertagnolli, E., Level set approach for the simulation of focused ion beam processing on the micro/nano scale. *Nanotech.* **2007,** 18, (26), 265307.

6. Kim, H.-B.; Hobler, G.; Lugstein, A.; Bertagnolli, E., Simulation of ion beam induced micro/nano fabrication. *J. Micromech. Microeng.* **2007,** 17, (6), 1178.

7. Stoyanov, S.; Bailey, C.; Tang, Y.; Marson, S.; Dyer, A.; Allen, D.; Desmulliez, M., Computational modelling and optimisation of the fabrication of nano-structures using focused ion beam and imprint forming technologies. *J. Phys. Conf. Ser.* **2010,** 253, 012008.

8. Mahady, K. T.; Tan, S.; Greenzweig, Y.; Raveh, A.; Rack, P. D., Simulating advanced focused ion beam nanomachining: a quantitative comparison of simulation and experimental results. *Nanotech.* **2018,** 29, (49), 495301.

9. Krizhevsky, A.; Sutskever, I.; Hinton, G. E., ImageNet classification with deep convolutional neural networks. *Commun. ACM* **2017,** 60, (6), 84-90.

10. LeCun, Y.; Bengio, Y.; Hinton, G., Deep learning. *Nature* **2015,** 521, (7553), 436-44.

11. Goodfellow, I.; Bengio, Y.; Courville, A., *Deep Learning*. MIT Press: 2016.

12. Mills, B.; Grant-Jacob, J. A., Lasers that learn: The interface of laser machining and machine learning. *IET Optoelectron.* **2021,** 15, (5), 207-224.

13. Ma, W.; Liu, Z.; Kudyshev, Z. A.; Boltasseva, A.; Cai, W.; Liu, Y., Deep learning for the design of photonic structures. *Nat. Photon.* **2021,** 15, 77-90.

14. Piccinotti, D.; MacDonald, K. F.; Gregory, S. A.; Youngs, I.; Zheludev, N. I., Artificial Intelligence for Photonics and Photonic Materials. *Rep. Prog. Phys.* **2021,** 84, 012401.

15. Amey, J. L.; Keeley, J.; Choudhury, T.; Kuprov, I., Neural network interpretation using descrambler groups. *Proc. Natl. Acad. Sci.* **2021,** 118, (5).

16. Mills, B.; Heath, D. J.; Grant-Jacob, J. A.; Eason, R. W., Predictive capabilities for laser machining via a neural network. *Opt. Express* **2018,** 26, (13), 17245-17253.

17. Heath, D. J.; Grant-Jacob, J. A.; Xie, Y.; Mackay, B. S.; Baker, J. A.; Eason, R. W.; Mills, B., Machine learning for 3D simulated visualization of laser machining. *Opt. Express* **2018,** 26, (17), 21574-21584.

18. McDonnell, M.; Grant-Jacob, J.; Xie, Y.; Praeger, M.; Mackay, B.; Eason, R.; Mills, B., Modelling laser machining of nickel with spatially shaped three pulse sequences using deep learning. *Opt. Express* **2020,** 28, (10), 14627-14637.

19. Mills, B.; Heath, D. J.; Grant-Jacob, J. A.; Xie, Y.; Eason, R. W., Image-based monitoring of femtosecond laser machining via a neural network. *J. Phys. Photon.* **2018,** 1, (1), 015008.

20. Xie, Y.; Heath, D. J.; Grant-Jacob, J. A.; Mackay, B. S.; McDonnell, M. D.; Praeger, M.; Eason, R. W.; Mills, B., Deep learning for the monitoring and process control of femtosecond laser machining. *J. Phys. Photon.* **2019,** 1, (3), 035002.

21. Zhang, Q.; Wang, Z.; Wang, B.; Ohsawa, Y.; Hayashi, T., Feature Extraction of Laser Machining Data by Using Deep Multi-Task Learning. *Information* **2020,** 11, (8), 378.

22. Stockman, M. I.; Kneipp, K.; Bozhevolnyi, S. I.; Saha, S.; Dutta, A.; Ndukaife, J.; Kinsey, N.; Reddy, H.; Guler, U.; Shalaev, V. M.; Boltasseva, A.; Gholipour, B.; Krishnamoorthy, H. N. S.; MacDonald, K. F.; Soci, C.; Zheludev, N. I.; Savinov, V.; Singh, R.; Groß, P.; Lienau, C.; Vadai, M.; Solomon, M. L.; Barton III, D. R.; Lawrence, M.; Dionne, J. A.; Boriskina, S. V.; Esteban, R.; Aizpurua, J.; Zhang, X.; Yang, S.; Wang, D.; Wang, W.; Odom, T. W.; Van Hulst, N. F.; Kling, M., Roadmap on Plasmonics. *J. Opt.* **2018,** 20, 043001.

23. Luk'yanchuk, B. S.; Zheludev, N. I.; Maier, S. A.; Halas, N. J.; Nordlander, P.; Giessen, H.; Chong, C. T., The Fano resonance in plasmonic nanostructures and metamaterials. *Nat. Mater.* **2010,** 9, 707-715.

24. Qiu, C.-W.; Zhang, T.; Hu, G.; Kivshar, Y., Quo Vadis, Metasurfaces? *Nano Lett.* **2021,** 21, 5461-5474.

25. Fan, M.; Andrade, G. F.; Brolo, A. G., A review on the fabrication of substrates for surface enhanced Raman spectroscopy and their applications in analytical chemistry. *Anal. Chim. Acta* **2011,** 693, (1-2), 7-25.

26. Hugall, J. T.; Singh, A.; van Hulst, N. F., Plasmonic Cavity Coupling. *ACS Photon.* **2018,** 5, (1), 43-53.

27. Isola, P.; Zhu, J.-Y.; Zhou, T.; Efros, A. A. In *Image-to-Image Translation with Conditional Adversarial Networks*, Proceedings of the IEEE Conference on Computer Vision and Pattern Recognition, 2017; pp 1125-1134.

28. Mirza, M.; Osindero, S., Conditional generative adversarial nets. **2014**, arXiv:1411.1784.

29. Zhang, H.; Sindagi, V.; Patel, V. M., Image De-Raining Using a Conditional Generative Adversarial Network. *IEEE T. Circ. Syst. Vid.* **2019,** 30, (11), 3943-3956.

30. Jha, D.; Ward, L.; Paul, A.; Liao, W.-k.; Choudhary, A.; Wolverton, C.; Agrawal, A., ElemNet: Deep Learning the Chemistry of Materials From Only Elemental Composition. *Sci. Rep.* **2018,** 8, (1), 17593.

31. Schleder, G. R.; Padilha, A. C. M.; Acosta, C. M.; Costa, M.; Fazzio, A., From DFT to machine learning: recent approaches to materials science–a review. *Journal of Physics: Materials* **2019,** 2, (3), 032001.

32. Feng, S.; Fu, H.; Zhou, H.; Wu, Y.; Lu, Z.; Dong, H., A general and transferable deep learning framework for predicting phase formation in materials. *NJP Computational Materials* **2021,** 7, (1), 10.

33. Ge, M.; Su, F.; Zhao, Z.; Su, D., Deep learning analysis on microscopic imaging in materials science. *Materials Today Nano* **2020,** 11, 100087.

34. Jumper, J.; Evans, R.; Pritzel, A.; Green, T.; Figurnov, M.; Ronneberger, O.; Tunyasuvunakool, K.; Bates, R.; Žídek, A.; Potapenko, A.; Bridgland, A.; Meyer, C.; Kohl,

S. A. A.; Ballard, A. J.; Cowie, A.; Romera-Paredes, B.; Nikolov, S.; Jain, R.; Adler, J.; Back, T.; Petersen, S.; Reiman, D.; Clancy, E.; Zielinski, M.; Steinegger, M.; Pacholska, M.; Berghammer, T.; Bodenstein, S.; Silver, D.; Vinyals, O.; Senior, A. W.; Kavukcuoglu, K.; Kohli, P.; Hassabis, D., Highly accurate protein structure prediction with AlphaFold. *Nature* **2021,** 596, (7873), 583-589.

35. Iten, R.; Metger, T.; Wilming, H.; Del Rio, L.; Renner, R., Discovering Physical Concepts with Neural Networks. *Phys. Rev. Lett.* **2020,** 124, (1), 010508.
36. Wu, T.; Tegmark, M., Toward an artificial intelligence physicist for unsupervised learning. *Phys. Rev. E* **2019,** 100, (3), 033311.
37. Raissi, M., Deep Hidden Physics Models: Deep Learning of Nonlinear Partial Differential Equations. *J. Mach. Learn. Res.* **2018,** 19, (1), 932-955.

TABLE OF CONTENTS IMAGE

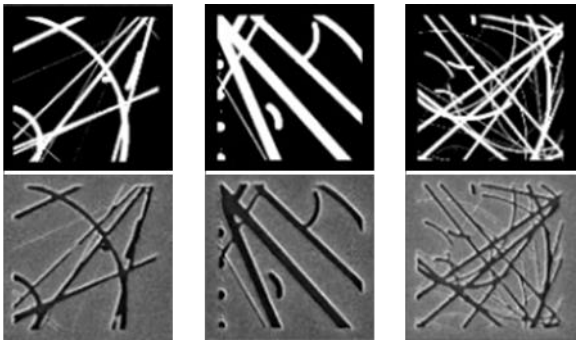

Deep Learning-Assisted Focused Ion Beam Nanofabrication

Oleksandr Buchnev[*], James A. Grant-Jacob[*], Robert W. Eason[*], Nikolay I. Zheludev[* †], Ben Mills[*], and Kevin F. MacDonald[*]

** Optoelectronics Research Centre, University of Southampton, Highfield, Southampton, SO17 1BJ, UK*

† Centre for Disruptive Photonic Technologies & The Photonics Institute, SPMS, Nanyang Technological University Singapore, 637371, Singapore

Convolutional Neural Network (CNN) for predicting ion beam dose from sample SEM images

The CNN was constructed of four convolutional layers, each formed of batch normalization, ReLU (Rectified Linear Unit) and pooling processes[1-5], followed by a fully connected layer with a single regression output using a mean square error loss[5].

The network was trained on SEM images of chevrons milled with dosage values in the set [0.5, 1.0, 1.5, …. 17.5] mC/cm^2, cropped to 299×299 pixels with random vertical and horizontal shifts of ±15 pixels in the position of the chevron relative to the center of the frame. Training proceeded for 50 epochs, with a learning rate of 0.00005 and batch size of 8, taking 3 minutes on an NVIDIA RTX2070 GPU.

In more detail, the input image was 299×299×3, followed by convolutions of 8 of 3×3×3 (with stride of 1), 16 of 3×3×8 (with stride of 2), 32 of 3×3×16 (with stride of 1), and 32 of 3×3×32 (with stride of 1).

The CNN was then tested on SEM images of chevrons milled with dosage values in the set [0.25, 0.75, 1.25, … 17.25] mC/cm^2, cropped to 299×299-pixels, with each prediction taking 2.5 ms.

Conditional Generative Adversarial Network (cGAN) for simulation of FIB-milled sample SEM images

The cGAN was formed by an 8-layer generator and a 4-layer discriminator, with a L1 to discriminator loss ratio of 200, learning rate of 0.0002, and was trained for 5 epochs on an NVIDIA Titan Xp GPU (taking 45 hours).

The network was trained on a set of fifty-nine 355×355-pixel binary design (input) and corresponding FIB milled sample SEM (output) images, and detail of the ion gun aperture (beam current) setting used in sample fabrication (Figure 3).

The SEM images were recorded at 710×710 pixels with a resolution of 5 nm. These were then rescaled by a factor of two, to 355×355 pixels (with 10 nm pixel size), matching the pixilation of the binary designs.

The dataset was augmented through random cropping of the 355×355-pixel images down to 256×256 pixels.

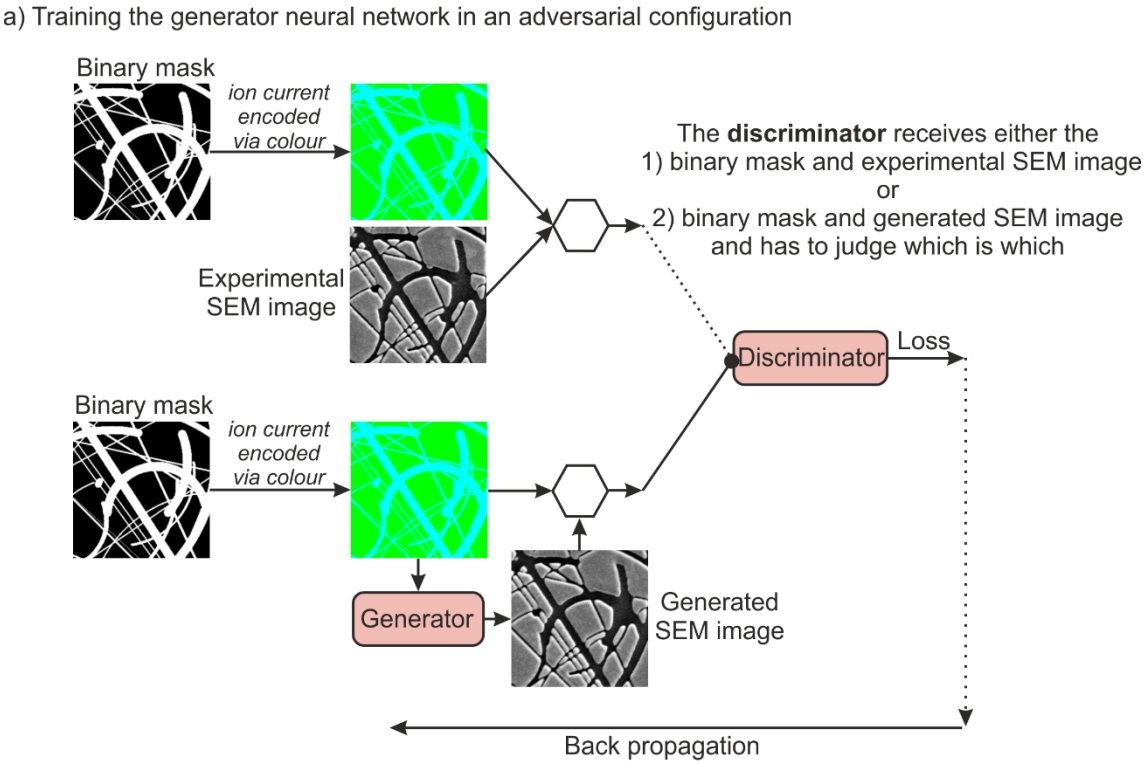

Figure S1. Schematic of the cGAN for adversarial training of the generator neural network used for predictive visualization.

After training, the cGAN was able to predict the appearance of a sample for any desired binary map, with each predictive visualization being computed in only 85 ms.

Figure S1 illustrates the training and application of the cGAN in more detail. Figure S1a shows a schematic of the generator and discriminator configuration, where the generator network transforms a binary mask into a generated SEM image, and the discriminator judges whether the generated SEM image appears experimental or generated. The expectation of this adversarial training approach is that, under appropriate conditions, the generator and discriminator networks become more effective over time.

In this work, the four different ion currents were included in the training data by changing the colour theme of the initial black-and-white binary masks, as shown in Fig. S1b.

As shown in Fig. S1c, once training was complete, the generator network could be used to transform any binary mask into a generated SEM image, i.e. as shown here, and in the manuscript, for transforming previously unseen binary mask images, which were not used during the training process.

References

1. Le, Q. V.; Jaitly, N.; Hinton, G. E. **2015**, arXiv:1504.00941v2.
2. Nair, V.; Hinton, G. E. In *Rectified Linear Units Improve Restricted Boltzmann Machines*, 27 th International Conference on Machine Learning, Haifa, Israel, 2010; Haifa, Israel.
3. Canziani, A.; Paszke, A.; Culurciello, E. **2016**, arXiv:1605.07678v4.
4. Chen, G.; Chen, P.; Shi, Y.; Hsieh, C.-Y.; Liao, B.; Zhang, S. **2019**, arXiv:1905.05928.
5. Miao, S.; Wang, Z. J.; Liao, R. *IEEE Transactions on Medical Imaging* **2016,** 35, (5), 1352-1363.